PAPER

Check for updates

Stretchable negative Poisson's ratio yarn for triboelectric nanogenerator for environmental energy harvesting and self-powered sensor†

Lijun Chen,‡[ab] Chaoyu Chen,‡[ab] Long Jin,‡[a] Hengyu Guo,[ac] Aurelia Chi Wang,[a] Fanggang Ning,[d] Qiaoli Xu,[ab] Zhaoqun Du,*[b] Fumei Wang*[b] and Zhong Lin Wang [ID] *[ae]

Due to the increasingly serious environmental pollution and the extreme shortage of energy resources, harvesting clean and sustainable random energy from the environment is a scientific, effective, and necessary solution in the coming intelligent era. Such random and disorder energy, like that from human motion and textile-related movement, can be obtained *via* textile-based triboelectric nanogenerators (TENGs). However, research related to textile-based TENGs with mature, high-efficiency, and economical manufacturing techniques is limited. Here, by using a high-speed ring spinning method, negative Poisson's ratio yarn (NPRY) with a composite structure is designed and fabricated as a variety of intelligent device. Based on the special negative Poisson's ratio effect, NPRY combined with TENG can be used as a foundation structure to form diverse flexible textile-based electronic devices, such as an energy harvesting fabric, a self-counting yoga elastic band, and a self-powered pre-alarm cable. At the same time, NPRY-TENGs with different structures and structural parameters are systematically investigated to optimize the output performance in this work. This special, low-cost, and highly efficient NPRY as a foundation structure material has promising applications in the manufacture of all kinds of textile-based TENGs and harvesting a lot of random energy from the environment, where the random energy can be used by other electronic devices or those textile-based TENGs themselves as self-powered sensors.

Broader context

Due to the increasingly serious environmental pollution and the extreme shortage of energy resources, harvesting clean and sustainable energy from the environment is a scientific, effective, and necessary solution in the coming intelligent era. At the same time, rapid development of the Internet of Things and intelligent disordered sensors requires more and more distributed sources. Obviously, conventional batteries are not the best choice for they have their own problems. So if random and sustainable energy, like that from human motion, can be obtained *via* textile-based triboelectric nanogenerators (TENGs), these problems may be solved or alleviated. Moreover, textile-based TENGs can be used as self-powered sensors to monitor human health and improve the quality of green and intelligent life. However, mature, highly efficient, and economical manufacturing techniques for textile TENGs are limited. Herein, we not only manufacture a negative Poisson's ratio composite yarn (NPRY) on a large scale, but also prove that the NPRY can be used as a foundation structure material to fabricate all kinds of textile-based TENGs for energy harvesting and self-powered sensors. Our systematic research has found that this special, low-cost and efficient NPRY has promising applications in sustainable and environmentally friendly intelligent devices.

[a] *School of Material Science and Engineering, Georgia Institute of Technology, Atlanta, GA 30332, USA. E-mail: zhong.wang@mse.gatech.edu*

[b] *Key Laboratory of Textile Science & Technology, Ministry of Education, College of Textiles, Donghua University, Shanghai 201620, P. R. China.*
 E-mail: wfumei@dhu.edu.cn, duzq@dhu.edu.cn

[c] *Department of Applied Physics, State Key Laboratory of Power Transmission Equipment & System Security and New Technology, Chongqing University, Chongqing 400044,*
 P. R. China

[d] *Industrial Research Institute of Nonwovens and Technical Textiles, College of Textiles and Clothing, Qingdao University, Shandong 266075, P. R. China*

[e] *Beijing Institute of Nanoenergy and Nanosystems, Chinese Academy of Sciences, Beijing 100083, P. R. China*

† Electronic supplementary information (ESI) available. See DOI: 10.1039/d0ee02777d

‡ C. C., L. C. and L. J. contributed equally to this work.

Introduction

In this era of rapid development of the Internet of Things and intelligent devices, mobile, wireless, and disordered sensors require more and more distributed sources. Energy storage devices such as batteries would be the first choice naturally. But batteries are not the best choice for their own problems, such as limited life time problem and recycling problem. Hence, the invention of triboelectric nanogenerators (TENG)[1] may solve this problem *via* replacing batteries. In recent years, because of environmental concerns and people's pursuit of a green and healthy life, TENGs have attracted long-lasting attention for their promising applications in converting ambient mechanical energy into electricity, which can be used for clean and sustainable power sources and portable self-powered sensors.[2–7] The mechanism of electron transfer and electrostatic induction effects[8–10] of TENGs makes it possible to convert almost all forms of motions into energy and electrical signals, which gives TENGs a broad application space from huge movement to minute ones, such as sea waves[11–13] and vessel pulsation.[14] Widely distributed across life, human motion is one of the most common dispersed and sustainable energies which can be easily harvested by wearable intelligent textiles.[15–17] At the same time, human health monitoring plays an increasingly important part in our daily life for an improved quality of life.[18,19] In addition, many textile-related movements in the natural environment can also be used to harvest energy.[20–23] Therefore, as a daily necessity for thousands of years, textiles can be the best medium for TENGs due to their ideal performance, such as low weight, breathability, and flexibility.

More and more researchers are paying attention to textile-based TENGs, including fiber-based TENGs, yarn-based TENGs, and fabric TENGs.[24–27] They have been applied to a lot of fields, ranging from biomechanical energy harvesting devices,[28,29] artificial electric skin,[30] and human-interactive interfaces[31] to wearable self-powered functional sensors.[32–35] However, textile-based TENGs still face challenges. Firstly, mass-manufactured textile-based TENGs with mature, high-efficiency, economical manufacturing techniques are limited. Some researchers have made progress in the scalable manufacture of yarn-based TENGs.[36] But their production speed is far less than that of conventional yarns from traditional spinning technology, such as the ring-spinning method. In addition, the production processes are somewhat complicated. Secondly, yarns are the foundation materials that can be used to fabricate diverse textiles. But the applications of most yarn-based TENGs are monotonous and limited. Thirdly, the gap distance of contact–separation mode of most stretchable yarn-based TENG sensors with core–shell structures is small and the mechanism is uncertain. A negative Poisson's ratio or auxetic material is a kind of special material because of its counterintuitive behavior of expanding transversely when it is stretched in the longitudinal direction.[37–40] Surrounded by other dielectric materials, contact–separation mode (the most stable and commonly used mode for TENGs) can easily be obtained under stretching situation.

Therefore, a negative Poisson's ratio material is a perfect choice for a stretchable TENG.

Herein, a negative Poisson's ratio yarn (NPRY) as a composite yarn which is made of thermoplastic polyurethane (TPU) yarn (core yarn) and polyamide (PA) conductive yarn (warping yarn) is designed and fabricated by a high-speed ring spinning method. Due to the high-efficiency, economical manufacturing technique, about 2000 meters of NPRY can be obtained about 1 hour on one ring bobbin, which can provide sufficient supply for industrial textile-based TENGs. As a foundation and secondary structure material, the NPRY can be used to form diverse textile based-TENGs, such as a self-powered stretchable fabric sensor, an energy harvesting fabric, a self-counting yoga elastic band, and a self-powered pre-alarm cable. Moreover, four fabric TENGs are fabricated to demonstrate that the NPRY is easily made into a more complicated structure for wearable devices. Twelve NPRY-TENGs with core–shell structure are fabricated to systematically investigate the influence of structure, materials, TPU yarn diameter, screw pitch, and length on the output performances and to optimize the design. All these results show that this special, low-cost and efficient NPRY has promising applications in sustainable and environmentally friendly intelligent devices.

Results and discussion

The deficiency of mature, highly efficient mass manufacturing technology has greatly hindered the development of textile-based TENGs. In order to solve this problem, we present here a traditional, mature spinning technique to fabricate a stretchable NPRY for use in a textile TENG, as shown in Fig. 1. For the NPRY, a polyamide (PA) yarn coated with Ag is used as the conductive electrode because of its high conductivity (Fig. 1A). PA yarn is also a very commonly used textile material worldwide, which has a high production and excellent performance such as high breaking strength, elongation, and abrasive resistance. According to previous work about negative Poisson's ratio,[39,40] to obtain a negative Poisson's ratio, this PA conductive yarn with small diameter and high tensile modulus is chosen as the wrapped yarn which is helically wound around a core yarn (elastic yarn, not limited to a particular material) with good elasticity and larger diameter, as shown in Fig. 1B.

In Fig. 1C, the spinning frame and fabrication process of the NPRY are clearly shown as a schematic illustration. PA conductive yarn and elastic yarn are moving from the bobbins, joining in the twisting triangle, and collected by a spinning tube. The components of the spinning frame in Fig. 1C are correspondingly marked in the physical photograph in Fig. S1A (ESI†). An enlarged view of the spinning tube is shown in Fig. S1B (ESI†). By moving the tension disc and guide mouth horizontally, the distance "*d*" can be adjusted in the top view of the spinning frame, Fig. S2 (ESI†). Then the intersection angle "*θ*" will change in twist triangle. Combined with the spinning speed, the structural parameters of the NPRY can be adjusted according to requirements. Based on this high-speed
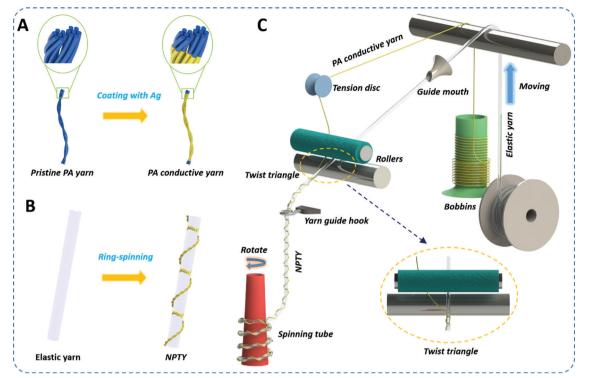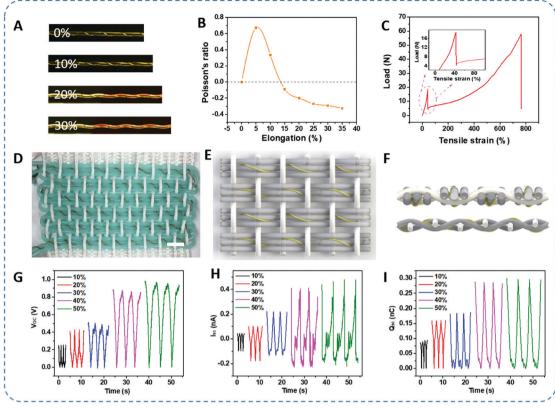
Fig. 1 Schematic illustration of the fabrication process of the NPRY. (A) Fabrication process of PA conductive yarn. (B) Schematic illustration of NPRY fabricated by elastic yarn. (C) Mass manufacture process of NPTY by ring spinning technology on a spinning frame. The inset in the lower right corner is an enlarged view of the twist triangle.

spinning technology (as shown in Movie S1, ESI†), in just one hour of operation, about 2000 meters of NPRY can be achieved from only one spinning tube. This greatly reduces the production cost (the estimate of raw material cost is shown in Table S1 and Note S1, ESI†) and promotes the wide application of textile-based TENGs.

As shown in Fig. 2A, the appearance of a typical NPRY is clearly presented when this NPRY is stretched from 0% to 30%. This NPRY is made of a two-ply twisted PA conductive yarn and TPU yarn. The physical photograph, scanning electron microscope image, and tensile property of PA conductive yarn are shown in Fig. S3 (ESI†). According to the schematic illustrations and photographs of changes in yarn shape in Fig. S4 and S5 (ESI†), PA conductive yarn and TPU yarn will exchange their positions in the inner and outer layers when the NPRY is stretched. That is, PA conductive yarn can change its position from the outer layer to the inner layer, which is the major structural feature of the NPRY. And it is also the direct influencing factor affecting the overall energy harvesting performance of NPRY based TENG, because this allows PA conductive yarn to contact and separate with external materials periodically. At the same time, the diameter of the whole yarn changes. The Poisson's ratio of the NPRY is calculated according to Note S2 (ESI†). As shown in Fig. 2B, it is a typical Poisson's ratio–elongation curve, as for most NPRYs, where Poisson's ratio is positive at the beginning, and then negative. This means that the diameter of the NPRY decreases firstly and then increases as the elongation increases. The tensile property of the NPRY is

shown in Fig. 2C. The inset in Fig. 2C shows the breaking point of the conductive PA yarn. Obviously, the NPRY partially broke twice. The first one is for PA conductive yarn (the inset in Fig. 1C), and the second one is for TPU yarn at a very high tensile strain of about 800%. This kind of NPRY has very good flexibility which is shown in Fig. S6 (ESI†). It could withstand arbitrary complex deformations, such as bending and distortion.

As textile materials, to make the fabric style devisable to satisfy the aesthetic requirements of the public, some kinds of NPRYs and NPRY fabric TENGs are fabricated, as shown in Fig. S5 and S7 (ESI†). In these fabric TENGs, NPRY is placed between two other kinds of yarns and then these three yarns are treated as a whole weft yarn to weave a fabric.

As shown in Fig. 2D, an NPRY which is made of four-ply twisted PA conductive yarn and silicone rubber yarn is woven into an NPRY fabric TENG. Schematic illustrations of the structure of this NPRY fabric TENG from different perspectives are shown in Fig. 2E (top view) and F (right view and front view). When this fabric is stretched in the weft direction, the PA conductive yarn will transfer from the outer layer into the inner layer, and the yarns beside the NPRY will be pushed away (Fig. S8A, B, E and F, ESI†). The working mechanism is shown in Fig. S8C, D, H and I, and Note S3 (ESI†). Cross-sections of the NPRY in the un-stretched situation and the stretched situation are shown in Fig. S8C-ii, S8D-ii, S8H-ii and S8I-ii (ESI†). As shown in Fig. 2G–I, the output performance V_{OC} (open-circuit voltage) I_{SC} (short-circuit current), and Q_{SC} (short-circuit charge transfer) will increase when increasing the elongation from

Fig. 2 The mechanical behavior of NPRY and output performance of NPRY fabric TENG. (A) Photographs of the NPRY under increasing elongation from 0% to 30%. (B) Representative Poisson's ratio–elongation curve of the NPRY. (C) Typical stress–strain curves of the NPRY. (D) Photograph of a fabric TENG made with the NPRY; scale bar 1 cm. (E and F) Schematic illustration of the structure of NPRY fabric TENG from different perspectives, including (E) top view and (F) right view and front view. (G to I) Electrical output of NPRY fabric TENG under stretch mode from 10% to 50%, including (G) V_{OC}, (H) I_{SC}, and (I) Q_{SC}.
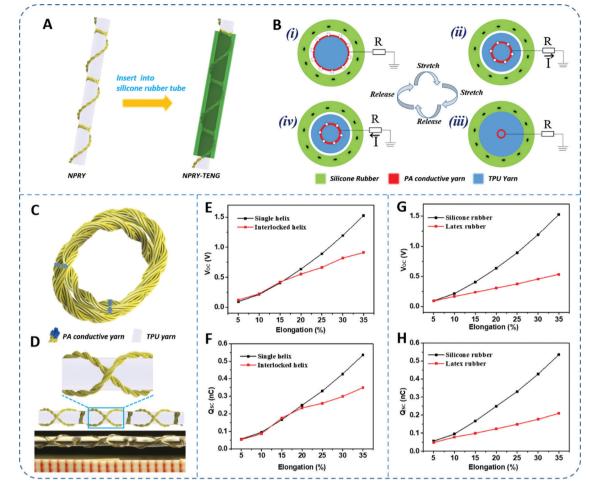
10% to 50%. Therefore, this NPRY fabric TENG can be used as a stretchable sensor to detect human motion.

As shown in Fig. 3A, by inserting the NPRY into a silicone rubber tube, a yarn TENG (NPRY-TENG) was manufactured. This unique helical auxetic structure endows the NPRY-TENG with good properties for generating electricity by stretching itself. During stretching, the diameter of the silicon rubber tube decreases slightly while increasing the diameter of the inner NPRY, as shown in Fig. S4 and S9 (ESI†). Here, the working mechanism of the NPRY-TENG during stretching mode is briefly demonstrated in Fig. 2B, which is based on a conjunction of triboelectrification and electrostatic induction. This stretching mode belongs to single-electrode mode.

Under stretching mode, in the original stage, the surfaces of the PA conductive yarn and the silicon rubber tube are charged with the same amount of opposite charges (Fig. 3B-i). The PA conductive yarn proves to be negatively charged because of the silicon rubber's ability to attract electrons.[41] By stretching this yarn TENG, the warp yarn (PA conductive yarn) straightens and transfers from the outer layer into the inner layer. This indicates that the PA conductive yarn gets separated from the silicon rubber tube. On the contrary, TPU is in contact with the silicon rubber tube. In this process, PA conductive yarn and the silicon rubber tube separate from each other. Positive

charges in the electrode (conductive yarn) will be induced by the negative charges, yielding an electron flow from the ground through external loading to the electrode (Fig. 3B-ii). As these two surfaces are moving quite far away, a new electrical equilibrium is achieved and the electrons stop moving (Fig. 3B-iii). On removal of the tensile strain, if the wrapped yarn (PA conductive yarn) or core yarn (TPU) is elastic, both yarns will recover to the initial starting configuration gradually. The PA conductive yarn approaches the silicone rubber tube again, and electrons flow in reverse from the electrode (PA conductive yarn) to the ground to achieve a charge balance (Fig. 3B-iv). When the PA conductive yarn contacts the silicone rubber tube, charge neutralization occurs again. Continuous contact–separation movements between the PA conductive yarn and the silicone rubber tube generate continuous alternating current outputs from the NPRY-TENG through the external loading.
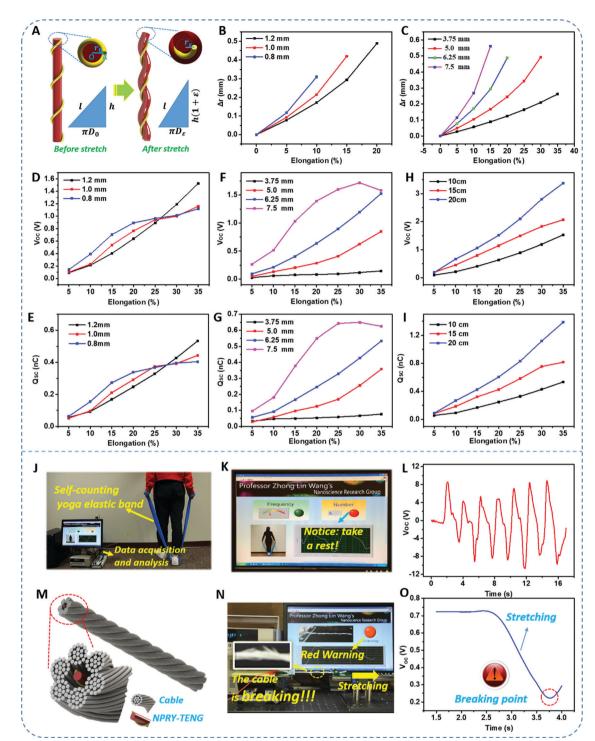
The electrical output performances are measured by using a linear motor to provide periodic contact–separation movements. To obtain a more quantitative understanding of the electricity generating process, we establish a theoretical model of the NPRY-TENG to observe the electric potential distribution of the PA conductive yarn and the silicone rubber tube during the contact–separation movements by a simple finite element simulation using COMSOL Multiphasic (Fig. S10B, ESI†).

Fig. 3 The working mechanism and electrical output performances of the NPRY-TENG. (A) Fabrication process of NPRY-TENG. (B) Schematic diagrams of the working principle of the NPRY-TENG under stretch. (C and D) Schematic illustration and photograph of interlocked helix structure of NPRY-TENG, including (C) transverse cross-section and (D) lateral view. (E and F) Electrical output performances of the NPRY-TENGs with two different structures (single helix structure and interlocked helix structure) under stretch, including (E) V_{OC} and (F) Q_{SC}. (G and H) Electrical output performances of the NPRY-TENGs fabricated by two different materials (silicon rubber tube and latex rubber tube) under stretch, including (G) V_{OC} and (H) Q_{SC}.

To investigate the effects of the structure on the electrical output performance, an interlocked helix structure NPRY-TENG was made as shown in Fig. 3C, D, and Fig. S11 (ESI†). Comparing with single helix structure NPRY (Fig. 3A), the outer layer is more stable. The cross-sections of this double wrapping yarn NPRY-TENG are presented in Fig. 3C and Fig. S11A (ESI†). In order to show the structure clearly, one of the outer layer yarns is represented in red in Fig. S11A (ESI†). The side views from different angles are shown in Fig. 3D and Fig. S11B (ESI†). All other structural parameters (such as test condition and length) of single helix structure and interlocked helix structure NPRY-TENGs are the same. The output performances are shown in Fig. 3E, F, and Fig. S12A–F (ESI†). Comparing these results, we find that the NPRY-TENG with the single helix structure has higher output. This is because, according to Fig. S13 and Note S4 (ESI†), for the NPRY-TENG with interlocked helix structure, only the intersection area is an effective contact area between PA conductive yarn and silicone rubber tube. But for the NPRY-TENG with single helix structure, the entire PA yarn can make contact with and separate from the silicone rubber effectively. So

the single helix structure is better than the interlocked helix structure. Latex rubber tube as elastic material was chosen for NPRY-TENG to investigate the influence of materials on the output performance as shown in Fig. 3G, H, and Fig. S12G–I (ESI†). It is obvious that NPRY-TENG with silicone rubber tube has better performance.

Here, a range of NPRY-TENGs with single helix structure and silicone rubber tube have been manufactured and tested to systematically study the influence of structural parameters on the output performance when these NPRY-TENGs are stretched from 5% to 35%. The results are presented in Fig. 4. Shown in Fig. 4A is a schematic illustration of the structure deformation of NPRY when the PA yarn spreads along the cylinder (TPU yarn) before and after stretch. According to eqn (8) in Note S5 (ESI†), for different structural parameters (different diameter D_{TPU} and different helix pitch h) we can calculate the variation "Δr" of r when increasing the elongation ε, as shown in Fig. 4B and C. In Fig. 4B, when the elongation and the helix pitch ($h =$ 6.25 mm) are the same, Δr of NPRY with minimum diameter ($D_{TPU} = 0.8$ mm) is the biggest. That is, for NPRY-TENG with a

Fig. 4 The electrical output performances of NPRY-TENGs with different structural parameters and applications of NPRY-TENG under stretch mode. (A) Schematic illustration of NPRY when the PA yarn spreads along the cylinder (TPU yarn) before and after stretch. (B) Δr of NPRYs with different diameter (0.8 mm, 1.0 mm, and 1.2 mm). (C) Δr of NPRYs with different helix pitches (3.75 mm, 5.0 mm, 6.25 mm, and 7.5 mm). (D and E) Electrical output performances of NPRY-TENGs with different diameters (0.8 mm, 1 mm, and 1.2 mm) of TPU yarn, including (D) V_{OC} and (E) Q_{SC}. (F and G) Electrical output performances of NPRY-TENGs with different helix pitches (3.75 mm, 5 mm, 6.25 mm, and 7.5 mm), including (F) V_{OC} and (G) Q_{SC}. (H and I) Electrical output performances of NPRY-TENGs with different lengths (10 cm, 15 cm, and 20 cm), including (H) V_{OC} and (I) Q_{SC}. (J) Demonstration of the NPRY-TENG as a self-counting yoga elastic band. (K) An intelligent test interface of a computer. (L) The V_{OC} of the self-counting yoga elastic band when the tester stretched it. (M) Schematic illustration of NPRY-TENG wrapped by cables. (N) Demonstration of the NPRY-TENG as a self-powered pre-alarm cable. (O) A typical V_{OC} curve when the self-powered pre-alarm cable is stretched and broken.

smaller D_{TPU}, the PA conductive yarn will be farther away from the tube when the elongation and the helix pitch h are the same. In Fig. 4C, when the elongation and the diameter (D_{TPU} = 1.2 mm) are the same, Δr of NPRY with maximum helix pitch (h = 7.5 mm) is the biggest. That is, for NPRY-TENG with bigger helix pitch h in Fig. 4A, the PA conductive yarn will be farther away from the tube when the elongation and the diameter D_{TPU} are the same.

For the accuracy of the test, when we investigate the influence of the diameter of TPU yarn, the helix pitch, the length, and test condition are the same in Fig. 4D, E and Fig. S14 (ESI†). Comparing the outputs of NPRY-TENGs, the NPRY-TENG with minimum diameter (D_{TPU} = 0.8 mm) has the biggest output when the elongation is the same and smaller than 25%, which is consistent with the result in Fig. 4B. However, when the elongation is larger than 25%, the NPRY-TENG with maximum diameter (D_{TPU} = 1.2 mm) has the biggest output. In theory, according to eqn (9) and (10) in Note S5 (ESI†), NPRY-TENGs with different diameters have different Δr_{max} and ε_{max}. The NPRY-TENG with the biggest diameter (D_{TPU} = 1.2 mm) has the biggest Δr_{max} and ε_{max}. According to Note S6 (ESI†), in practice, PA yarn is not a rigid body, the NPRY-TENGs can be still stretched and Δr will increase to the biggest value slowly and then decrease when the PA conductive yarn is basically straight. Hence, the outputs V_{OC} and Q_{SC} of NPRY-TENGs (D_{TPU} = 0.8 mm and 1.0 mm) still increase slowly when elongation is bigger than 25%. For the whole stretch process, compared with the outputs of NPRY-TENG (D_{TPU} = 0.8 mm and 1.0 mm), the outputs of NPRY-TENG (D_{TPU} = 1.2 mm) maintain a more stable growth trend for both V_{OC} and Q_{SC}.
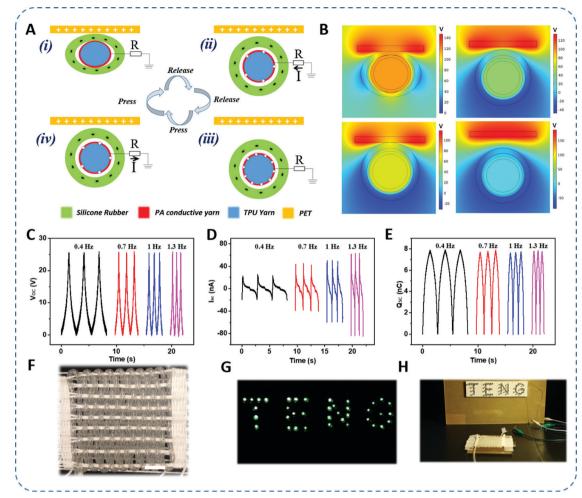
When we investigate the influence of helix pitches, the other parameters and test conditions are also kept the same in Fig. 4F, G, and Fig. S15 (ESI†). We can draw a simple conclusion that the outputs increase with increasing helix pitch from 3.75 mm to 7.5 mm which is basically consistent with the results in Fig. 4C. However, when the helix pitch is bigger than 6.25 mm, the outputs of NPRY-TENG will reach the maximum value when the elongation is very small (25% for NPRY-TENG with a helix pitch of 7.5 mm), and then decrease when elongation increases. This is because the V_{OC} and Q_{SC} of NPRY-TENG will first increase to the maximum and then decrease with elongation increasing (Note S6, ESI†). And the larger the helix pitch, the smaller the elongation of the PA conductive yarn when it is basically straight (D_ε = 0, and Δr is a maximum, Note S5, ESI†). Hence, a helix pitch of 6.25 mm is the best choice here. In addition, the stress–strain curves of NPRY with different helix pitches are shown in Fig. S16 (ESI†). As we can see in Fig. 4H, I and Fig. S17 (ESI†), NPRY-TENGs with different lengths (other parameters are the same) were tested. It is obvious that the outputs will increase with increasing length from 10 cm to 20 cm. The outputs of NPRY-TENG are presented in Fig. S18 (ESI†) when it is stretched under different frequencies. The V_{OC} and Q_{SC} will decrease slightly, and the I_{SC} will increase significantly when increasing the frequency from 0.5 Hz to 2 Hz. According to the results in Fig. 4, it can be summarized that this NPRY-TENG can be used as a self-powered stretching sensor.

Moreover, the stability of a NPRY-TENG was tested as shown in Fig. S19 (ESI†). Under the test conditions of 15% elongation and 0.2 Hz frequency, the V_{OC} is 0.545 V at the beginning and remains at 59% (0.322 V) of the original output after stretching continuously for 6.5 hours, about 4800 times. This shows that the NPRY-TENG has relatively good tensile fatigue resistance. Moreover, the V_{OC} can be restored to 88% (0.480 V) of the original output after the stretching stops for 12 hours, which presents its great elastic recovery performance.

According to the good output performances of NPRY-TENG under the stretch mode, it can be used as a self-powered stretchable sensor by harvesting human biomotion energy. As shown in Fig. 4J–L, a long NPRY-TENG (about 1.5 meters) was fabricated and attached to a yoga elastic band as a self-counting yoga elastic band. By stretching this yoga elastic band, it can detect and record the frequency and number in real time when doing physical exercise. As shown in Movie S2 (ESI†), the stretching frequency of the tester is about 0.5 Hz. A stretching number can be set to remind the tester to have a rest. Here when the tester stretches the yoga elastic band more than 6 times, a grey button in the monitoring interface from the computer will turn to red (Fig. 4K). The electrical signal obtained by the computer is shown in Fig. 4L. So by using this self-powered sensor without extra power like batteries, the tester can precisely control the speed and amount of exercise to avoid physical injury caused by excessive exercise. In addition, the NPRY-TENG can be used as a self-powered pre-alarm cable by replacing the silicone rubber tube with other yarns or cables (Fig. 4M). As shown in Fig. 4N, O and Movie S3 (ESI†), when this self-powered pre-alarm cable is stretched and broken, the voltage immediately stopped falling and began to increase in the reverse direction. Then the grey button will turn red (red warning), which gives a signal to change the cable. And at the same time, the NPRY and other cables will continue to withstand the tension which offers precious time to deal with this incident. If the breaking of the cable were to be dangerous to life, this self-powered sensor would be significantly helpful because one would have time to escape.

After the NPRY was inserted into a silicone rubber tube to form the NPRY-TENG, this NPRY-TENG can be treated as weft yarn alone to weave a plain fabric TENG (NPRY-TENG fabric). When this NPRY-TENG fabric is pressed by other things such as PET or human hands, it can be used to harvest human motion energy or other similar environmental energy. As shown in Fig. 5A, the working mechanism of this NPRY-TENG fabric is presented. In the original stage, no electrical potential exists between the surface of the silicone rubber tube and PET film. By pressing PET film onto the fabric, the surfaces of the silicone rubber tube and PET film are charged with the same amount of opposite charges (Fig. 5A-i). The silicone rubber tube proves to be negatively charged because of the silicon rubber's ability to attract more electrons than the PET film. When they are separated from each other, positive charges will be induced in the electrode (PA conductive yarn) by the negative charges, yielding an electron flow from the Ag through external loading to the ground (Fig. 5A-ii). As the PET film moves quite far away,

Fig. 5 Working mechanism and electrical output performance of the NPRY-TENG fabric under compression mode. (A) Schematic diagrams of the working principles of the NPRY-TENG. (B) Simulated electric field distribution of the NPRY-TENG. (C to E) Electrical output performances of a fabric manufactured with NPRY-TENG fabric at different press frequencies, including (C) V_{OC}, (D) I_{SC}, and (E) Q_{SC}. (F) Photograph of NPRY-TENG fabric; scale bar 1 cm. (G) Demonstration of lighting up LEDs marked with letters "TENG" by tapping the NPRY-TENG fabric with the hands. (H) Photograph of NPRY-TENG connecting with LEDs.

a new electrical equilibrium is achieved and the electrons stop moving (Fig. 5A-iii). As the PET film approaches the silicone rubber tube again, electrons flow in reverse from the ground to the electrode (PA conductive yarn) to achieve a charge balance (Fig. 5A-iv). When the PET film fully contacts the silicone rubber tube, charge neutralization occurs again. Continuous contact–separation movements between the PET film and the silicone rubber tube generate continuous alternating current outputs from this NPRY-TENG fabric through the external loading. The electrical output performances are measured by using a linear motor to provide periodic contact–separation movements. To obtain a more quantitative understanding of the electricity generating process, we establish a theoretical model of the fabric TENG to observe the electric potential distribution of PET film and NPRY-TENG during the contact–separation movements by a simple finite element simulation using COMSOL Multiphasic (Fig. 5B). The V_{OC}, I_{SC}, and Q_{SC} of this mode are presented in Fig. 5C–E when the contacted area is 25 cm², and the press frequency increases from 0.4 Hz to

1.3 Hz. The V_{OC} and Q_{SC} remain almost the same and the I_{SC} increases significantly with increasing frequency. Fig. 5F–H show that this fabric TENG can sufficiently light up "TENG" letters with 38 LEDs in series by bare hand tapping (Movie S4, ESI†). By weaving this flexible fabric TENG into clothing, carpet, or curtain, we can easily harvest clean and sustainable mechanical energy to power lights or intelligent devices.

Conclusions

In summary, a NPRY which is made of PA conductive yarn and elastic yarn is designed to fabricate NPRY fabric TENG and NPRY-TENG. Based on a high-speed ring spinning technology, in just one hour of operation, about 2000 meters of NPRY can be achieved from only one spinning tube. This greatly reduces the production cost and can promote the wide application of textile-based TENGs. Due to the special negative Poisson's ratio effect, the NPRY combined with two other yarns can be treated as a whole weft yarn to weave an NPRY fabric TENG, which can

be used as a self-powered wearable and stretchable sensor. Then, by inserting the NPRY into a silicone rubber tube, an NPRY-TENG is fabricated and systematically investigated. This NPRY-TENG can not only be used for fabricating an energy-harvesting fabric TENG but also can be used as a self-counting yoga elastic band to monitor human motion. Furthermore, the NPRY-TENG can be used as a self-powered pre-alarm cable to offer precious response time to deal with incidents. This mass-manufactured NPRY acting as the foundation and secondary structure material for TENG fabrication provides a promising research orientation for clean power sources and self-powered sensors of textile-based TENGs.

Experimental

Preparation of the negative Poisson's ratio yarn

A PA yarn coated with Ag (Jameco Electronics Inc.) is chosen as the warping yarn and conductive electrode, and TPU yarn is chosen as the core yarn. Firstly, as shown in Fig. 1C, the TPU yarn with large diameter is pulled out from a bobbin and then passes through the guide mouth and rollers. The PA conductive yarn is also pulled out from another bobbin and then passes through the tension disc and rollers. Secondly, after passing through the yarn guide mouth, these two yarns are tied together and fixed on the spinning tube. Thirdly, after setting the operating parameters of the spinning frame, the spinning tube will rotate at high speed. Then PA conductive yarn will wrap around the TPU yarn regularly.

Preparation of silicone rubber yarn

Silicone rubber (Mold Star 15 Slow, Smooth-On Inc.) is prepared by mixing its two components (Part A and Part B) in a 1:1 weight ratio, and then the silicone rubber is mixed with PDMS (Sylgard 184 Silicone Elastomer Base, Dow Corning Inc.) in a 3:1 weight ratio. The mixture is put into a vacuum to eliminate bubbles. Then, the mixture is injected into the plastic tube. The silicone rubber yarn will be obtained after the mixture is cured in an oven for 30 minutes at 60 degrees. At last, the plastic tube is peeled off.

Fabrication of the fabric TENG

All the fabric TENGs in this paper are fabricated by a self-designed mold. This self-designed mold was manufactured by imitating mature weaving technology which has existed in the textile field for a long time. The warp yarn (cotton yarn) is wound around the self-designed mode with dozens of rows which depends on the width of the required fabric. The weft yarn (NPRY, NPRY-TENG, or silicone rubber yarn) is interwoven with the warp yarns.

Characterization and measurements

The NPRY was fabricated by a ring spinning machine. The surface morphology of the silver-coated PA yarn was characterized by a field emission scanning electron microscope (SU-8010, Hitachi). The mechanical tensile test was conducted by a universal mechanical testing machine (Instron 5567). The electrical outputs (V_{OC}, I_{SC}, and Q_{SC}) of the TENG during compressing and stretching operations were implemented by a linear motor and an electrometer (Keithley 6514 System). The compressing forces were measured by a Vernier LabQuest Mini.

Conflicts of interest

There are no conflicts to declare.

Acknowledgements

References

1 F.-R. Fan, Z.-Q. Tian and Z. L. Wang, *Nano Energy*, 2012, **1**, 328–334.
2 Z. L. Wang, *ACS Nano*, 2013, **7**, 9533–9557.
3 G. Liu, H. Guo, S. Xu, C. Hu and Z. L. Wang, *Adv. Eng. Mater.*, 2019, **9**, 1900801.
4 L. Zhang, B. Zhang, J. Chen, L. Jin, W. Deng, J. Tang, H. Zhang, H. Pan, M. Zhu and W. Yang, *Adv. Mater.*, 2016, **28**, 1650–1656.
5 Z. Wen, Y. Yang, N. Sun, G. Li, Y. Liu, C. Chen, J. Shi, L. Xie, H. Jiang and D. Bao, *Adv. Funct. Mater.*, 2018, **28**, 1803684.
6 Z. Wen, M. H. Yeh, H. Y. Guo, J. Wang, Y. L. Zi, W. D. Xu, J. N. Deng, L. Zhu, X. Wang, C. G. Hu, L. P. Zhu, X. H. Sun and Z. L. Wang, *Sci. Adv.*, 2016, **2**, e1600097.
7 W. Zhang, P. Wang, K. Sun, C. Wang and D. Diao, *Nano Energy*, 2019, **56**, 277–285.
8 Z. L. Wang and A. C. Wang, *Mater. Today*, 2019, **30**, 34–51.
9 Z. L. Wang, *Faraday Discuss.*, 2014, **176**, 447–458.
10 W. Zhang, D. Diao, K. Sun, X. Fan and P. Wang, *Nano Energy*, 2018, **48**, 456–463.
11 Z. Wu, H. Guo, W. Ding, Y.-C. Wang, L. Zhang and Z. L. Wang, *ACS Nano*, 2019, **13**, 2349–2356.
12 Z. L. Wang, *Nature*, 2017, **542**, 159.
13 X. Liang, T. Jiang, G. Liu, Y. Feng, C. Zhang and Z. L. Wang, *Energy Environ. Sci.*, 2020, **13**, 277–285.
14 W. Fan, Q. He, K. Meng, X. Tan, Z. Zhou, G. Zhang, J. Yang and Z. L. Wang, *Sci. Adv.*, 2020, **6**, eaay2840.
15 J. Kim, S. Byun, S. Lee, J. Ryu and S. Hong, *Nano Energy*, 2020, **75**, 104992.
16 N. Soin, T. H. Shah, S. C. Anand, J. Geng, W. Pornwannachai, P. Mandat, D. Reid, S. Sharma, R. L. Hadimani and D. V. Bayramol, *Energy Environ. Sci.*, 2014, **7**, 1670–1679.
17 J. Ryu, J. Kim, J. Oh, S. Lim, J. Y. Sim, J. S. Jeon, K. No, S. Park and S. Hong, *Nano Energy*, 2018, **55**, 348–353.
18 S. Majumder, T. Mondal and M. J. Deen, *Sensors*, 2017, **17**, 130.

19 X. W. Wang, Z. Liu and T. Zhang, *Small*, 2017, **13**, 1602790.

20 Q. Jiang, B. Chen and Y. Yang, *ACS Appl. Energy Mater.*, 2018, **1**, 4269–4276.

21 Z. Zhao, X. Pu, C. Du, L. Li, C. Jiang, W. Hu and Z. L. Wang, *ACS Nano*, 2016, **10**, 1780–1787.

22 W. Seung, H. O. Yoon, T. Y. Kim, M. Kang and S. O. Kim, *Adv. Funct. Mater.*, 2020, 2002401.

23 J. Q. Xiong, M. F. Lin, J. X. Wang, S. L. Gaw, K. Parida and P. S. Lee, *Adv. Eng. Mater.*, 2017, **7**, 1701243.

24 X. He, Y. Zi, H. Guo, H. Zheng, Y. Xi, C. Wu, J. Wang, W. Zhang, C. Lu and Z. L. Wang, *Adv. Funct. Mater.*, 2017, **27**, 1604378.

25 J. Wang, X. Li, Y. Zi, S. Wang, Z. Li, L. Zheng, F. Yi, S. Li and Z. L. Wang, *Adv. Mater.*, 2015, **27**, 4830–4836.

26 X. Pu, L. X. Li, M. M. Liu, C. Y. Jiang, C. H. Du, Z. F. Zhao, W. G. Hu and Z. L. Wang, *Adv. Mater.*, 2016, **28**, 98.

27 M. Zhu, Y. Huang, W. S. Ng, J. Liu, Z. Wang, Z. Wang, H. Hu and C. Zhi, *Nano Energy*, 2016, **27**, 439–446.

28 J. Chen, Y. Huang, N. Zhang, H. Zou, R. Liu, C. Tao, X. Fan and Z. L. Wang, *Nat. Energy*, 2016, **1**, 16138.

29 C. Chen, H. Guo, L. Chen, Y.-C. Wang, X. Pu, W. Yu, F. Wang, Z. Du and Z. L. Wang, *ACS Nano*, 2020, **14**, 4585–4594.

30 P. S. Das and J. Y. Park, *Electron. Lett.*, 2016, **52**, 1885–1886.

31 Y. C. Lai, J. Deng, S. L. Zhang, S. Niu, H. Guo and Z. L. Wang, *Adv. Funct. Mater.*, 2017, **27**, 1604462.

32 C. Chen, L. Chen, Z. Wu, H. Guo, W. Yu, Z. Du and Z. L. Wang, *Mater. Today*, 2020, **32**, 84–93.

33 K. Dong, Z. Wu, J. Deng, A. C. Wang, H. Zou, C. Chen, D. Hu, B. Gu, B. Sun and Z. L. Wang, *Adv. Mater.*, 2018, **30**, 1804944.

34 Z. Lin, Z. Wu, B. Zhang, Y. C. Wang, H. Guo, G. Liu, C. Chen, Y. Chen, J. Yang and Z. L. Wang, *Adv. Mater. Technol.*, 2019, **4**, 1800360.

35 F. Shahmiri, C. Chen, A. Waghmare, D. Zhang, S. Mittal, S. L. Zhang, Y.-C. Wang, Z. L. Wang, T. E. Starner and G. D. Abowd, *Proceedings of the 2019 CHI Conference on Human Factors in Computing Systems*, 2019.

36 W. Gong, C. Hou, J. Zhou, Y. Guo, W. Zhang, Y. Li, Q. Zhang and H. Wang, *Nat. Commun.*, 2019, **10**, 868.

37 R. Lakes, *Science*, 1987, **235**, 1038–1040.

38 J. R. Wright, M. R. Sloan and K. E. Evans, *J. Appl. Phys.*, 2010, **108**, 044905.

39 M. R. Sloan, J. R. Wright and K. E. Evans, *Mech. Mater.*, 2011, **43**, 476–486.

40 S. Liu, X. Pan, D. Zheng, Z. Du, G. Liu and S. Yang, *Text. Res. J.*, 2019, **89**, 1003–1012.

41 H. Zou, Y. Zhang, L. Guo, P. Wang, X. He, G. Dai, H. Zheng, C. Chen, A. C. Wang and C. Xu, *Nat. Commun.*, 2019, **10**, 1427.